American Mineralogist, Volume 72, pages 451–467, 1987

Chalcopyrite disease in sphalerite: Pathology and epidemiology[1]

Paul B. Barton, Jr., Philip M. Bethke
Mail Stop 959, U.S. Geological Survey, Reston, Virginia 22092, U.S.A.

Abstract

Blebs of chalcopyrite have been widely recognized in sphalerite from most sulfide deposits for as long as ore microscopy has been practiced. All too often they have been casually attributed to exsolution, whereas, in fact, many probably originate by replacement. In this descriptive paper we identify three widely occurring textures (designated as "watermelon," "dusting," and "bimodal") that characterize the disease; these are clearly the result of replacement of original Fe-bearing sphalerite by an aggregate of chalcopyrite and low-Fe sphalerite as an integral part of the mineralization process. However, the replacement interpretation involves an unresolved paradox because it requires extensive solid-state diffusion in materials that also retain sharp compositional gradients and thereby give evidence for minimal solid-state diffusion. Replacement probably predominates over alternative modes of origin for small chalcopyrite blebs in sphalerite from most vein and sea-floor massive sulfide deposits that formed in the 200–400°C range and that have not been subsequently subjected to higher temperatures. Mississippi Valley–type deposits do not show any of the three textures.

In addition to above-mentioned ailments, sphalerite from the epithermal silver-lead-zinc deposit at Creede, Colorado, displays a rich variety of features (given as a group the designation "bead chains") that are almost surely primary crystal dislocations decorated by exsolved chalcopyrite. The bead chains show strong preference for Fe-rich sphalerite. The fact that not all crystals, or even all equally Fe-rich sectors of sector-zoned crystals, show the bead chains suggests that disequilibrium distribution of Cu may play an important role in bead-chain development.

Introduction

Sphalerite is probably the most useful mineralogical guide to the processes of ore deposition. It is common in a wide variety of deposit types; it is transparent (except when very Fe rich), allowing for excellent three-dimensional textural study; it exhibits a variety of colors that provide visual indications of growth morphologies; it is a good host for fluid inclusions; it is relatively refractory so that initial conditions are preserved; and it has calibrated phase relations (specifically the amount of FeS in solid solution) that permit it to provide useful chemical parameters that help reconstruct the chemical environment of mineralization.

With all of these desirable characteristics, surely Murphy's law would require that some defect must be present, and there is one—the susceptibility to the ailment that is the topic of this communication.

In the summer of 1959 we, accompanied by Ed Roedder, Marc Bodine, and Norman Page, began a protracted study of the epithermal silver-lead-zinc veins at Creede, Colorado. Soon thereafter we began to examine conventional polished sections and noted the common occurrence of textures such as that illustrated in Figure 1.

Figure 1 shows a uniform field of sphalerite containing irregularly distributed blebs of chalcopyrite. We were aware that the sphalerite was color banded; what could be a more logical conclusion than that some of the bands became supersaturated on cooling and exsolved chalcopyrite, just as the textbooks said? But that conclusion soon proved to be a problem. Experimental work that Pete Toulmin and one of us (Barton) were then doing on sphalerite sensitized us to the extremely sluggish rates of solid-state reaction that prevented effective experimentation below about 600°C (it required more than a year to reverse solid-state reactions). That knowledge, combined with the facts that the Creede ores were formed at temperatures of less than 300°C, are only 25 m.y. old, and have never been metamorphosed or even deeply buried, made exsolution an unattractive proposition.

Not long thereafter we began to examine doubly polished thin sections, imitating the procedure used by Ed Roedder to study fluid inclusions. The features that had initially been observed in reflected light (Fig. 2a, and also Fig. 1) were revealed in transmitted light (Fig. 2b) to consist of a complex and heretofore undescribed texture. It has a core of coarse, vermicular chalcopyrite intergrown with essentially colorless sphalerite that is surrounded by

[1] Adapted from the Presidential Address of Paul B. Barton, Jr., at the annual meeting of the Mineralogical Society of America, November 11, 1986, in San Antonio, Texas.

0003–004X/87/0506–0451$02.00

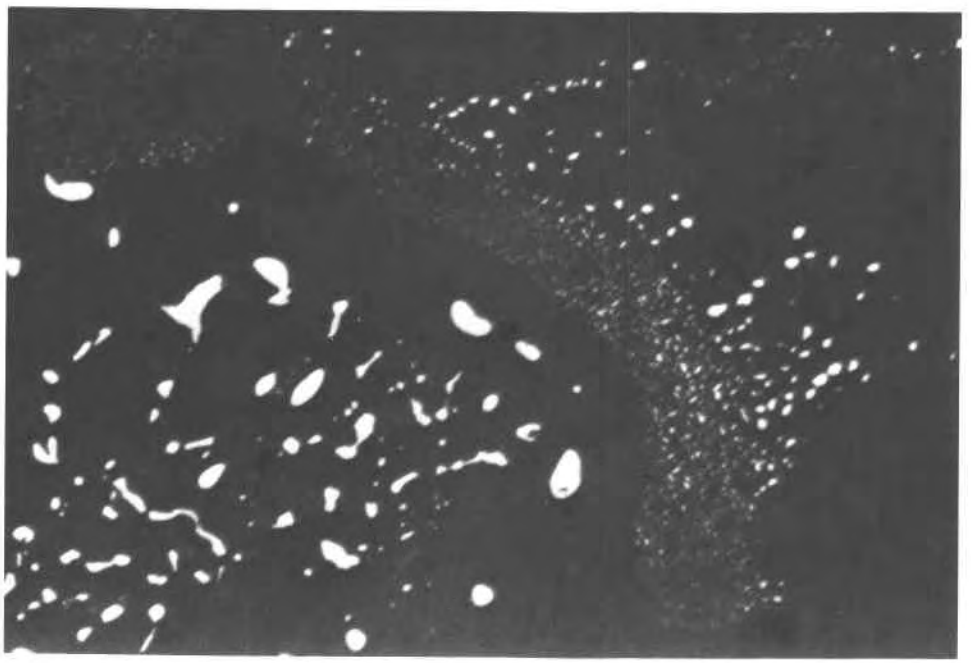

Fig. 1. Chalcopyrite (light) in a single crystal of sphalerite (dark), photographed in reflected light (oil immersion) showing varying sizes and irregular distribution of chalcopyrite blebs. Field width, 0.022 mm; specimen PBB (4) from Creede, Colorado.

a nearly chalcopyrite-free zone of colorless sphalerite. The core is very sharply bounded by sphalerite with finer chalcopyrite intergrown so densely that it is opaque in even the thinnest sections (at least as thin as 20 μm); outward within a few micrometers, the opaque zone passes into the fresh, color-banded sphalerite. This, obviously, is not exsolution; but what is it?

About 1970 we showed this feature to Jim Craig. His response created a new descriptive term for ore petrology when he said, "That's not a texture; that's a disease!"; we have called it the "chalcopyrite disease" ever since. The first use of the term in print was in Barton's (1978) note on sphalerite from the Furutobe mine, Japan, and the phrase has since become widely adopted. However, a diagnosis yielding only the name for a disease is not very satisfying; the real questions are what is it and how did it originate? We hope that some readers might find an interesting and challenging tidbit or two for further investigation.

Before we examine the chalcopyrite disease proper, let us see what some fresh, *healthy* sphalerite looks like.

An unusually simple, tiny part of a typical healthy sphalerite crystal with no visible chalcopyrite from Creede is shown in Figure 2f. Figure 3 presents the composition of the sphalerite based on microprobe traverse along the narrow, straight, vertical line on Figure 2f. In this and subsequent traverses, points were analyzed by 10-s counts every 4 μm. It should be clear that the colored bands on Figure 2f correspond to the Fe peaks on Figure 3. Note that the Fe content is shown as a solid line and the Cu content as a dashed curve. The quantitative measure of the Fe content is mole percent FeS, even though some of the Fe (particularly in the other traverses) may be contained in chalcopyrite; this reflects the fact that all of the Fe was initially in the sphalerite. The quantitative measure of Cu is volume percent chalcopyrite; this is facilitated by the fact that the Cu content of the sphalerite is too low to measure and is done simply by assuming that the $Cu_{0.5}Fe_{0.5}S$ and (Zn,Fe)S have similar volumes. Pure chalcopyrite was used as the Cu standard and synthetic (Zn,Fe)S as Fe standards. The Cu content in Figure 3 is essentially at background. Nowhere in our microprobe study of natural materials formed at relatively low temperatures have we detected Cu in solid solution in sphalerite (i.e., Cu in sphalerite must be less than ~0.1%); when we detect Cu, we see Cu minerals. Synthetic sphalerite is a different matter, and at high temperature it can be prepared with much dissolved Cu.

Now let us note a few more undiseased sphalerites from a variety of deposits to show that the features we ascribe to healthy sphalerite from Creede are not particularly unusual. Figure 2g illustrates the core of a sphalerite crystal from the huge copper-silver-zinc deposit at Butte, Montana, showing nice banding, a little sector zoning and perhaps even an erosional disconformity wherein the outside of the paler yellow zone to the right is truncated by later brown sphalerite on the extreme right. Figure 2h is a crystal from the ophiolite-related copper deposits of Cyprus. Even though it originated as part of a submarine hydrothermal system, this sphalerite looks just like something from a vein in the American cordillera. Figure 2c is sphalerite from the Mississippi Valley deposits in Wisconsin; in this crystal aggregate, the strong compositional banding is made irregular by uneven crystallite development. We have not recognized the chalcopyrite disease from this type of deposit, but we show the specimen to demonstrate that complex crystal-growth banding is a typical feature of almost all low-temperature sphalerite deposits.

Finally Figure 2i is another specimen from Creede with complex growth banding. The color bands represent growth zones that index the chemical changes that occurred while the crystals grew.

Usually, the darker the bands, the higher the Fe content. FeS in solid solution *always* colors sphalerite. There are *also* some intensely colored sphalerites with low Fe, but we will not be concerned with them here.

With ideal materials and numerous samples, one may be able to correlate individual growth bands from place to place within the deposit and thereby generate a stratigraphy of sphalerite (for an excellent example, see McLimans and others, 1980). The entire stratigraphic assemblage for a deposit is seldom seen in a single sample, but must be reconstructed from many specimens. A typical deposit may have several hundreds or perhaps even thousands of visually distinguishable growth bands ranging right down to the limits of optical resolution, although usually only the coarser features are traceable widely within a deposit.

Because the solubility of sphalerite is so low, each growth band that is more than a few micrometers thick requires so much fluid to nourish it that the fluid filling the vein must have been replenished many times during the growth of that individual band. Thus the growth band provides a very narrow unequivocal time band, a time band so narrow that it is, for practical purposes, a time *line*. Such time lines are essential components to any attempt to establish instantaneous thermal or chemical gradients within an ore body.

Sphalerite deposition need not be continuous. It may be interrupted by chemical erosion and the development of microkarst that is subsequently buried by later crystal growth. Figure 2j shows remnants of an aggregate of yellow sphalerite crystals containing an Fe-rich, brown band; it has been deeply corroded and then subsequently refilled by colorless sphalerite that simply renewed growth in crystallographic continuity with the older sphalerite foundation. We bring up this aspect of the behavior of sphalerite to assure the reader that we can recognize corrosion disconformities and that the things we are discussing in terms of the chalcopyrite disease are *not* of this origin.

Watermelon texture

Now, let us return to the description of the disease. We refer to the texture shown in Figures 2a and 2b as "watermelon," with a "rind" of fine chalcopyrite enclosing a core of colorless sphalerite containing a central zone of coarse, vermicular "seeds" of chalcopyrite. This pair of photos shows only a restaurant-sized serving of watermelon, but a larger piece is provided in Figure 2d. The chalcopyrite in the rind ranges in size from a fraction of a micrometer up to 1 or 2 μm in diameter, too small to be seen clearly at this magnification.

Figure 5a shows unusually coarse and anhedral chalcopyrite in the outer rind passing gradually (to the left) into much finer chalcopyrite in the inner rind. In many specimens the chalcopyrite crystals in the rind are euhedral rather than rounded as shown here. A chalcopyrite-free zone is intermediate between the rind and the seedy core. In contrast to the rind, the chalcopyrite crystals making up the seeds are always anhedral, and individuals may be more than a hundred micrometers in longest dimension. We have not observed twinning in any of the blebs of chalcopyrite, and the seeds may well be single crystals. The chalcopyrite aggregate seems to radiate outward, and there is a strong resemblance to a myrmekitic intergrowth. In Figure 2d we see that the seedy zones outline the former positions of the initially Fe-rich bands in the primary sphalerite and that the rind is positioned as expected on the outside of the watermelon.

Often the whole specimen is severely modified, and the beautiful color banding destroyed. The specimen illustrated in Figures 2d and 2e is unusual in that it catches the process in middevelopment. If we could see *only* specimens of the sort of material shown in the upper left and upper right parts of Figure 2e, we would be hard pressed to discover the origin of the texture.

The low-Fe sphalerite is even less anisotropic than the original crystals, and what anisotropism exists is patchy in both original and new sphalerite. Thus we cannot make extensive use of optics to examine crystallographic relations. In a few instances, twinning passes undeflected through the watermelons, sometimes with the seeds being more concentrated along the twin planes. Some thin edges exhibit throughgoing cleavages that support the twinning evidence in showing that the secondary sphalerite is in crystallographic continuity with its monocrystalline host.

Figures 4 and 6, in conjunction with Figures 2d and 5a, respectively, reveal some quantitative aspects of the watermelon texture. In Figure 2d, three traverses are marked on the lower part of the photomicrograph; they correspond to the three microprobe tracings in Figure 4. Traverse C–C′ crosses an undiseased, Fe-rich growth band. Note that the Cu content is essentially nil. Traverse B–B′ just nips the edge of the rind of the watermelon, and here we note that the Cu content (recorded as volume percent chalcopyrite) has definitely increased. Also, note that the fineness of the texture is such that all analyzed spots showing appreciable Cu are composites of sphalerite + chalcopyrite. It is obvious that the Fe content of the sphalerite between the tiny chalcopyrite crystals within the rind is quite low, a few tenths of 1 mol% FeS at the most, because the sphalerite fluoresces blue-white in the electron beam. Traverse A–A′ cuts all of the components of the watermelon. Because so many of the chalcopyrite inclusions do not crop out on the polished surface (or are even within a few micrometers of the surface) the microprobe tracing shows comparatively few Cu-bearing spots. We see that the rind has now expanded into what was originally the lower-Fe sphalerite band. The new colorless sphalerite is uniformly low in Fe.

The seedy part of the watermelon is mostly low-Fe sphalerite with only a few chalcopyrite-bearing areas falling within the analyzed spots. Even the microprobed spots that are Cu-rich contain some of the low-Fe sphalerite

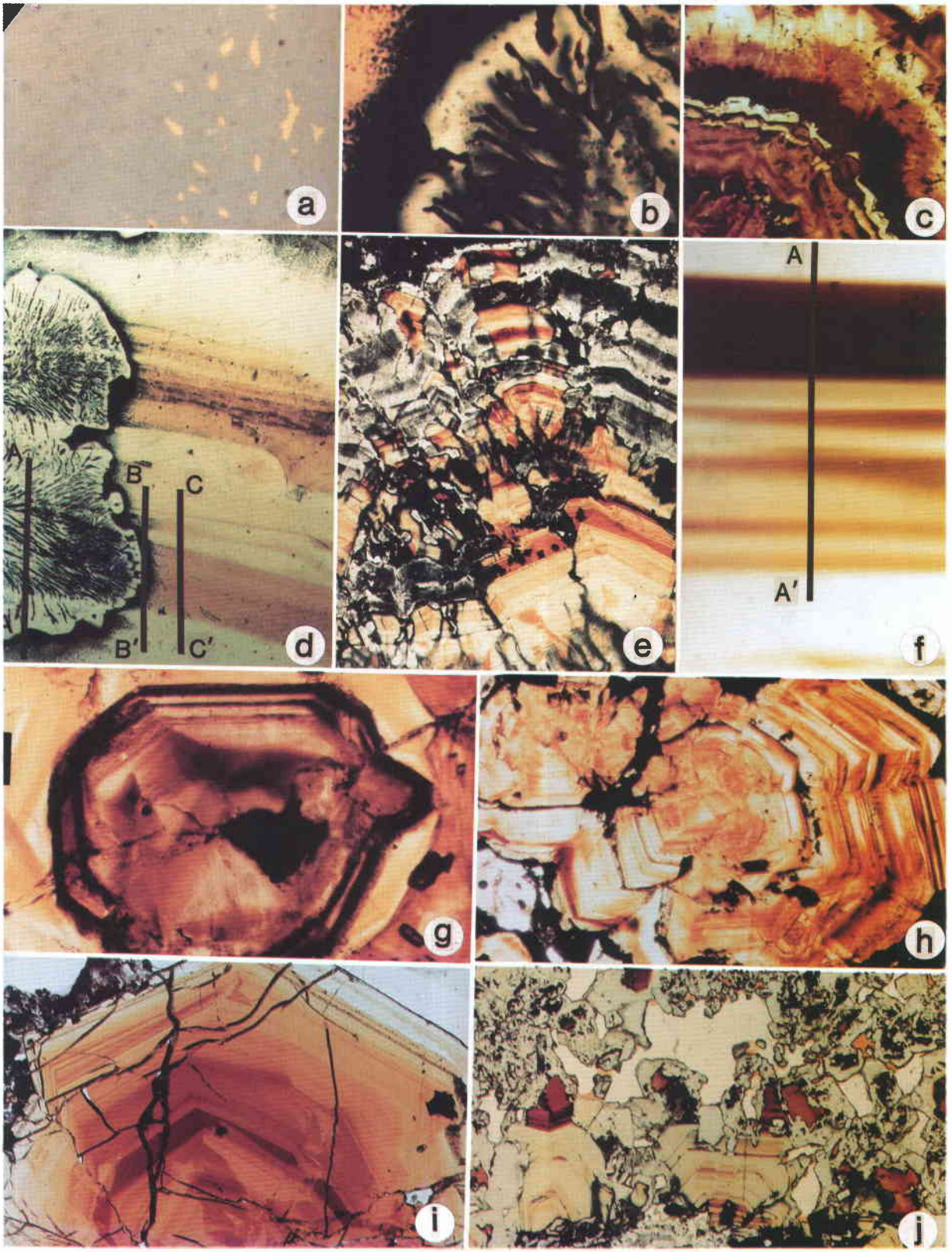
a
b
c
A
B
C
B′
C′
d
e
A
A′
f
g
h
i
j

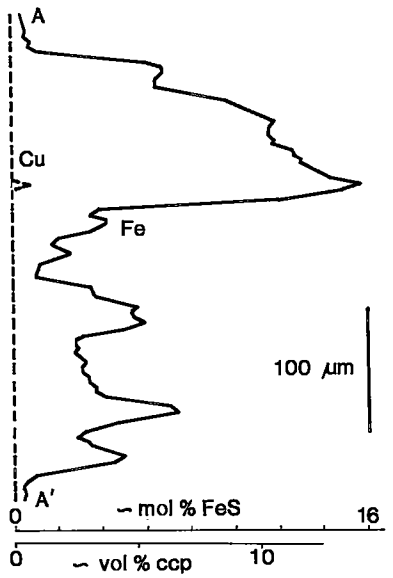

Fig. 3. Microprobe analyses for Fe and Cu along the traverse shown in Fig. 2f. Fe is plotted here in terms of mol% FeS (solid line) because the Fe was originally in sphalerite even though the Fe analyzed now resides in both sphalerite and chalcopyrite. Cu is plotted as vol% chalcopyrite (dashed line) to make comparison with photographs easier, and this approach is permissible because the sphalerite contains no detectable Cu in solid solution.

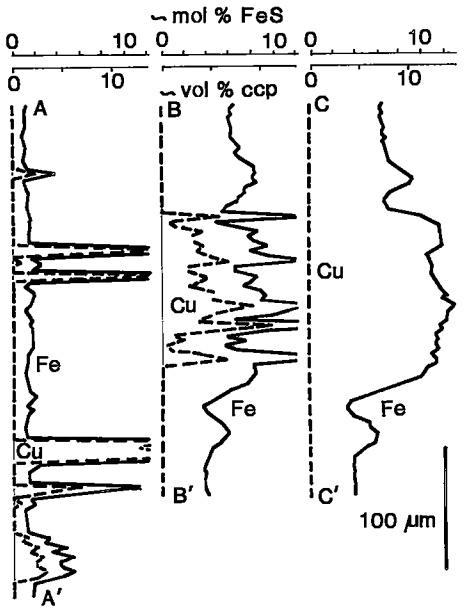

Fig. 4. Microprobe analyses for Fe and Cu along the traverses shown in Fig. 2d. Traverse A–A′ crosses all facies of the watermelon texture; B–B′ crosses only the rind; C–C′ is in unaltered banded sphalerite. Also, see caption for Fig. 3.

host, and they are still only a few volume percent chalcopyrite. The spotty character of this record provides horrendous sampling statistics so that we cannot use it to prove whether or not Fe is conserved as the watermelon develops. A few additional analyzed samples, plus the faithful preservation of the Fe-rich banding, do suggest, but not prove, that Fe is conserved in this process. However, we still have problems deciding where the Fe goes when the low-Fe, chalcopyrite-free zone forms between the Fe-bearing rind and Fe-bearing core and, also, what happens to the chalcopyrite in the rinds when adjacent watermelons coalesce.

In Figures 5a and 6 there is a second example with a pair of traverses that show another set of similar characteristics. In this example we have utilized a reflected-light photo as the sample map, and we have enlarged the

←

Fig. 2. Collage of color photomicrographs. (*a*) Chalcopyrite (yellow) blebs in a single crystal of sphalerite (gray). Reflected light (oil immersion); field width, 0.090 mm; specimen PBB (31) from Creede, Colorado. (*b*) Identical field to 2a, but in transmitted light. This example of the watermelon texture shows a seedy core of opaque, myrmekitic chalcopyrite inclusions on the right and a rind of an opaque chalcopyrite + sphalerite aggregate on the left. Undiseased sphalerite is in the upper left. (*c*) Typical banded sphalerite from a Mississippi Valley–type ore deposit. Transmitted light; field width, 2.75 mm; specimen from the North Hayden mine, Wisconsin. (*d*) Lower magnification of the watermelon texture of the same specimen as in Fig. 2a and 2b. The watermelon texture has encroached from the left into the undiseased, color-banded sphalerite. Three microprobe traverses are indicated by the three vertical black lines; the results of the analyses are plotted in Fig. 4. Field width, 0.70 mm; transmitted light. (*e*) Still lower magnification of same specimen as Figs. 2a, 2b, and 2d. Crystal aggregate of color-banded sphalerite shows partial replacement by colorless sphalerite + chalcopyrite. Fe-rich bands have yielded nearly opaque chalcopyrite-rich bands. At bottom of field, the dusting aspect of the chalcopyrite disease has apparently moved outward from grain boundaries. Field width, 7.0 mm; transmitted light. (*f*) Part of a simple, undiseased, color-banded sphalerite crystal. The vertical black line marks the position of the microprobe traverse plotted in Fig. 3. Transmitted light; field width, 0.250 mm; specimen PMG-BG from Creede, Colorado. (*g*) Core of a typical banded sphalerite crystal from the Leonard mine, Butte, Montana. The core of the crystal shows sector zoning. Transmitted light; field width, 0.90 mm. (*h*) Complexly color-banded sphalerite from an ophiolite-related, massive sulfide deposit. Transmitted light; field width, 2.0 mm; specimen from Skouriotissa mine, Cyprus, provided by J. J. Hemley. (*i*) Color-banded, partly sector-zoned, gemmy sphalerite. This specimen has many excellent bead chains illustrated in parts of Fig. 11. Transmitted light; field width, 50 mm; specimen PMB-AK from Creede, Colorado. (*j*) Sphalerite microkarst. The lower part of the specimen shows remnants of an outer dark-brown band. A solution disconformity has cut out much of the dark band and parts of the underlying lighter sphalerite; this was followed by deposition of unbanded, colorless sphalerite that backfilled the karst. Transmitted light; field width, 10 mm; specimen PMB-F from Creede, Colorado.

field to emphasize the watermelon analogy of the texture. The original sphalerite has Fe-rich banding oriented approximately horizontally across the field. Traverse A–A′ provides a cross section through the watermelon. Traverse B–B′ is a control from undiseased sphalerite of an equivalent stratigraphic position; it is dashed because the position shown is projected in from a traverse actually located off the figure to the right.

The thin curved lines in Figure 6 connecting traverse A–A′ with B–B′ indicate stratigraphically equivalent horizons. The area attacked by the disease lies *within* the principal Fe-rich band, *not* along its margin; the margins of the Fe-rich band are similar in each traverse, and the chalcopyrite is limited to the interior of the Fe-rich band. (Note that the plots shown in Fig. 6 extend well beyond the margins of Fig. 5a.) A thin, Fe-rich band near the top of the traverse has had chalcopyrite added also, but the band is too narrow to develop the characteristic watermelon pattern.

We have dozens of examples of the watermelon texture from Creede and one or two from the Kuroko deposits; in every instance, the scales of the textures are similar. Neither pygmy nor giant examples have been discovered.

We do not know how the watermelon texture develops; its transgressive nature proves that it cannot be the product of an original mixture of sphalerite and chalcopyrite, but instead it is certainly a secondary feature. All known examples (except those where the replacement has gone to completion) show the full sequence: (1) fresh sphalerite, (2) rind, (3) clear sphalerite without chalcopyrite, and (4) seedy core. Thus we are inclined to think that all four zones migrate as a unit, moving simultaneously outward from fractures into the healthy sphalerite, as Figures 2d and 2e strongly suggest. When watermelons coalesce, the rinds disappear, but the ghosts of the original Fe-rich bands are preserved, as shown in upper left and right parts of Figure 2e. The banding remains after all of the original sphalerite is lost, like the grin of Lewis Carroll's Cheshire Cat.

The watermelon texture is fascinating, but it is not the only symptom of the chalcopyrite disease. In fact, the watermelon texture is not universal in occurrence, but because it is so spectacular, we chose to use it as our first example. Of much more common occurrence than the watermelon is a simple "dusting" of fine chalcopyrite in sphalerite, the term being descriptive of the appearance, not the mode of formation.

Dusting of chalcopyrite in sphalerite

In Figures 5d and 5e we see how the chalcopyrite dusting has proceeded into the walls of a crack for a distance of 50 to 100 μm. The depth of penetration of this type of dusting is highly variable; eventually it envelopes the entire crystal, converting it to low-Fe sphalerite containing disseminated chalcopyrite. It is easy to visualize such a process from Figure 5f, which shows fractured sphalerite about half-way to complete alteration.

Figure 5c illustrates an infection of the dusted aspect of the chalcopyrite disease from the Iwami mine in Japan. It spreads outward into rather uniform sphalerite from a veinlet now filled by colorless sphalerite. Note in Figure 7 that the original Fe content is 2 to 3% FeS, and total Fe (in sphalerite plus that in chalcopyrite) possibly may remain constant right across the diseased grain margins, falling to a lower level along the late sphalerite filling. However, the Fe content *of the sphalerite host* for the chalcopyrite dusting does fall significantly. As with the watermelon, the counting statistics for irregularly spaced grains are terrible, so that average bulk compositions are not easily obtained, but Fe is probably conserved.

The chalcopyrite dusting is fine grained, ranging down from a very few micrometers to below the level of optical resolution. In transmitted light, some sphalerites have a smoky blue, or more rarely, a smoky green or yellow color that may well be due to particles of so fine a grain size that the aggregate appears blue—a grain diameter on the order of a few hundreths of 1 μm is about ¼ the wavelength of blue or green light in sphalerite. Figure 5i shows cloudly blue and greenish-yellow sphalerite from the Magma mine, Arizona; the sparse larger opaque specks are probably coarser chalcopyrite particles. We have also seen similar turbid colors from the Kuroko deposits of Japan; from the Lark mine adjacent to the Bingham, Utah, porphyry copper deposit; and from the gold mines of Central City, Colorado.

The dusting of chalcopyrite in sphalerite is an almost universal phenomenon in unmetamorphosed hydrothermal ores. Because none of the samples we have examined from a dozen Mississippi Valley–type deposits show it, the dusting is probably limited to deposits formed above perhaps 200°C.

Although dusting occurs widely in many sphalerite parageneses, it is common for the earlier sphalerite to be much more extensively infected than is later sphalerite. Quite often microkarst surfaces are highlighted by chalcopyrite dusting of the etched foundation, as if the corrosion event coincided with a period of infection by chalcopyrite dusting (see Barton, 1978, Fig. II-2). We feel confident that this type of chalcopyrite disease is a feature that develops at intervals *during,* rather than subsequent to, mineralization.

We have no evidence that either the dusting or watermelon formation involves any appreciable change in volume, there being neither shrinkage openings, cleavage cracks, nor disruption of banding along the margins of the infected regions.

We suggest that the dusting and watermelon syndromes are different aspects of the same process. The watermelon aspect develops when there are strongly contrasting compositional differences between adjacent bands in the primary sphalerite, and the simple dusting aspect occurs wherever the original sphalerite is not strongly compositionally banded. Figure 2e shows an example of such behavior with the upper 80% of the sphalerite in the field

of view having been converted to watermelon texture and the lower 20% having been simply dusted along grain boundaries.

Bimodal chalcopyrite disease

We have already uncovered a nest of problems, but there is an additional, and even more poorly understood, variant of the chalcopyrite disease. We refer to this one as the "bimodal" texture because it is characterized by an intergrowth of two highly contrasting populations (Fig. 5b). The first is low-Fe sphalerite so thickly intergrown with chalcopyrite that it is nearly opaque; the second is essentially chalcopyrite-free, low-Fe sphalerite. (Additional examples are given in Barton, 1978, Fig. I-3 and II-3.)

A microprobe tracing across the bimodal texture (Fig. 8) shows that the Fe content *of the sphalerite* is very low, regardless of whether it is in the chalcopyrite-rich or chalcopyrite-poor facies. The position of the traverse is indicated by the vertical line in Figure 5b. The low-Cu area at the very top corresponds to the clear sphalerite at the top of the traverse. Almost every other analyzed spot along this traverse has at least a trace of chalcopyrite, the only exceptions being the broader zones of white sphalerite where we see that the dashed line for chalcopyrite returns to the background level. Near A′ the traverse crosses a 20 × 30 μm crystal of chalcopyrite, showing what sort of signal results from pure chalcopyrite.

The distribution of the pale sphalerite septae is reminiscent of syneresis features associated with the shrinkage of colloids, although a colloidal origin seems completely incompatible with the sharply angled ghost-crystal bands shown in Figure 5b. Near the edges of thin sections where cleavage is developed during polishing, one commonly observes that the clear patches of sphalerite are in crystallographic continuity with the chalcopyritized opaque regions. The clear regions appear both along preexisting grain contacts and as cross-cutting features. Although we need additional evidence of gradations between them, the three end-member textures—watermelon, dusting, and bimodal, seem related. We have searched for, but have not identified, any instance where any one of the features crosscuts another; however, Figures 14, 22, 24, 26, and 27 in Eldridge and others (1983) show dusting that has attacked rather uniform sphalerite from Kuroko deposits in a way that suggests that the dusting may be a transition into the bimodal texture.

Pathogenesis of the chalcopyrite disease

The watermelon texture highlights a severe and unresolved paradox, and our reluctance to expose our ignorance to public scrutiny is one reason why we have waited so long to publish a description of it. On one hand the faithful reproduction of textures without the development of open space (see Fig. 2e) seems to demand a process dominated by solid-state diffusion. This would involve diffusion for distances measured in many tens, or even hundreds, of micrometers. But on the other hand, some of the same polished sections (of which Fig. 2e is also an excellent example) preserve original compositionally banded sphalerite that has not experienced enough solid-state diffusion to blur the original compositional gradients, even on a scale of a few micrometers. Thus we have strong evidence, both pro and con, in the same specimen, for significant solid-state diffusion. The dusting and bimodal textures share the same problem, but the evidence is not quite so blatantly contradictory.

The sharpest compositional changes in the sphalerite banding shown in Figures 3 and 6 correspond to about 0.1% change in cell edge over a distance of about 0.015 mm (about 30 000 unit cells). One might ask whether such change could create a stressed region favorable for diffusion, or perhaps a contrast in thermal expansion might contribute to the same effect. We must rule out both these possibilities because the zones favored for attack by the disease (see Figs. 2d and 5a) are not the compositionally steep interfaces where stress should be focused, but rather the Fe-rich zones as a whole.

Table 1 summarizes the general symptoms of the chalcopyrite disease, and Table 2 lists the principal processes we shall consider next.

We do not challenge the concept of co-deposition of chalcopyrite with sphalerite, but the textures of the chalcopyrite disease do *not* arise from co-deposition. We offer two illustrations, the first of which is problematic and the second a clear-cut example of what really *is* co-deposition.

The center of Figure 9a shows a single sloping sphalerite growth surface on which fine chalcopyrite (the black specks) may have nucleated epitaxially as the crystal grew upward and from right to left. Then the chalcopyrite crystals were buried. When this feature is developed best, the chalcopyrite is very regularly arrayed, suggesting an orchard of fruit trees, and we give these features the term "orchard texture." However, even this example is suspect because we note in the upper left part of Figure 9a that

Table 1. General symptoms of the chalcopyrite disease

1. Fe conserved overall, but diminished in the sphalerite
2. Cu added; Zn presumably lost
3. No volume change (possibly excepting biomodal aspect)
4. Crosscutting textures abundant
5. Fine textures of original sphalerite replaced
6. Solid-state diffusion minor

Table 2. Principal processes leading to sphalerite + chalcopyrite intergrowths

1. Simultaneous or alternating deposition
2. Exsolution from solid solution
3. Replacement
   A. Bulk
   B. Selective
4. Mechanical mixing
5. Subsequent recrystallization of types 1, 2, 3, and 4

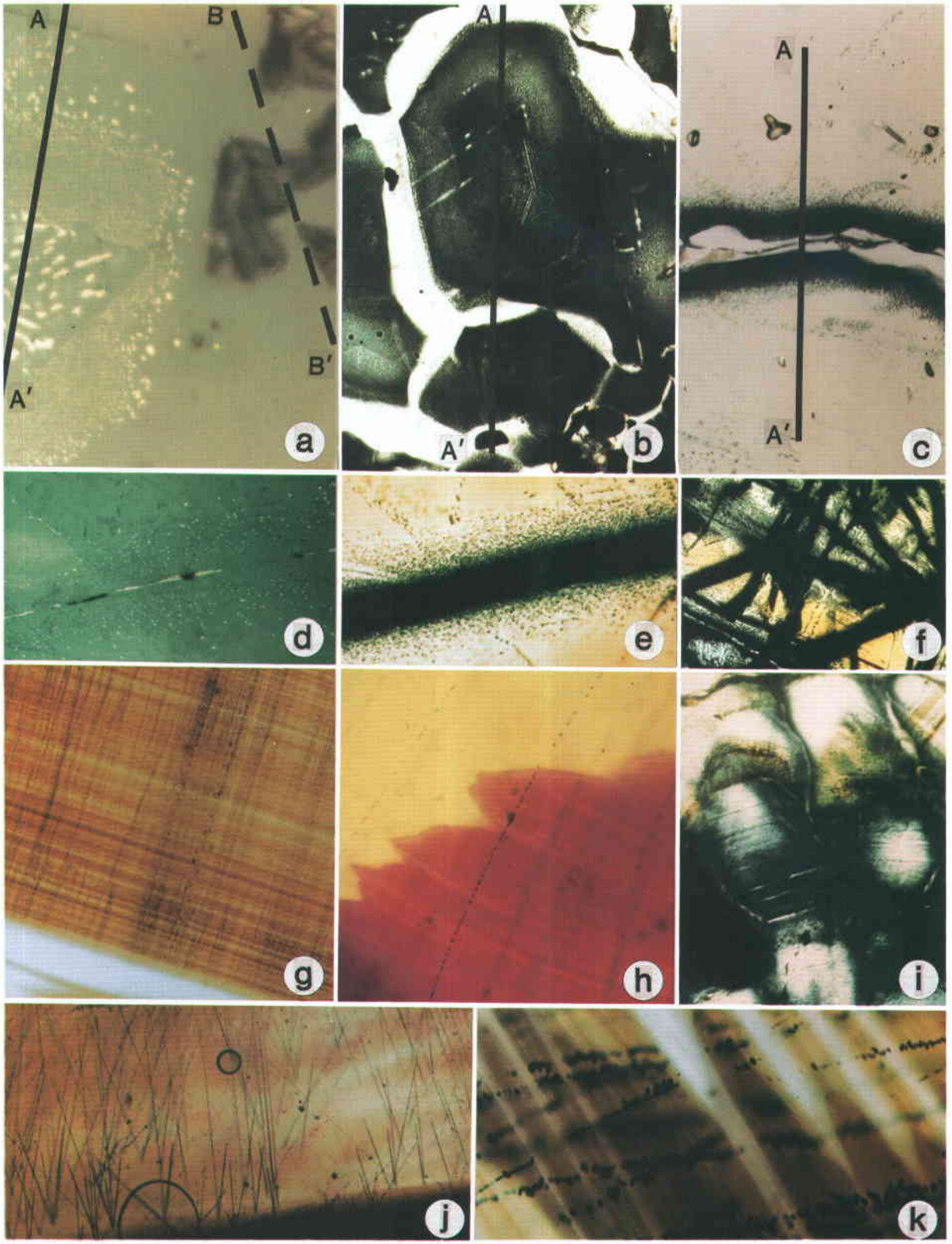
A
B
B′
A′
a
A
A′
b
A
A′
c
d
e
f
g
h
i
j
k

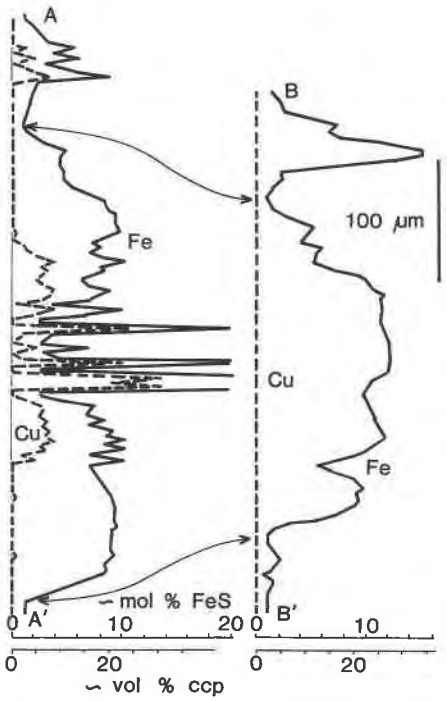

Fig. 6. Microprobe analyses for Fe and Cu along the traverses shown in Fig. 5a. Also, see caption for Fig. 3. Note that although the labels in Fig. 5a identify the traverses, only the central quarter of each traverse is present in the photograph, as explained in the caption for Fig. 5a.

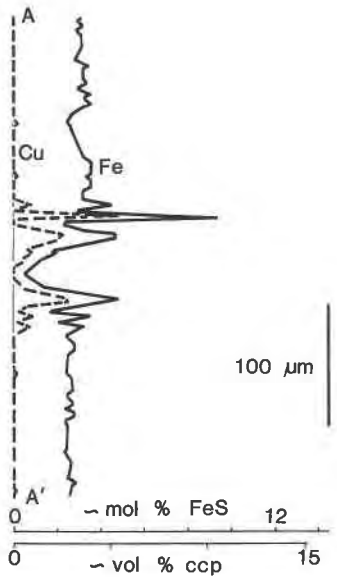

Fig. 7. Microprobe analyses for Fe and Cu along the traverse shown in Fig. 5c. Also, see caption for Fig. 3.

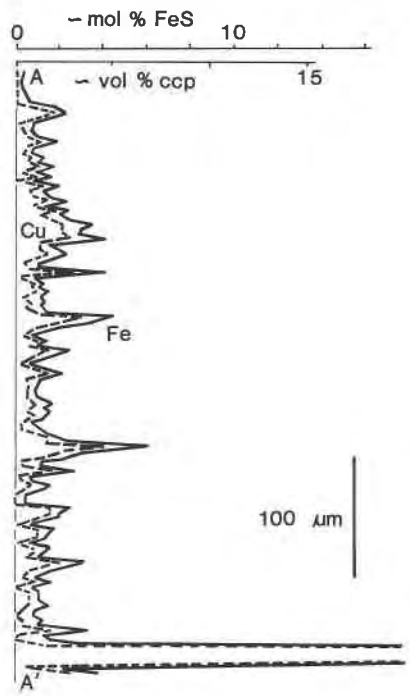

Fig. 8. Microprobe analyses for Fe and Cu along the traverse shown in Fig. 5b. Also, see caption for Fig. 3.

←

Fig. 5. Collage of color photomicrographs. (*a*) Detail of watermelon texture; reflected light (oil immersion). Black lines show position of microprobe traverses whose analyses are plotted in Fig. 6. In order to optimize the display of the watermelon, this figure corresponds *only* to the central 25% of the complete traverses plotted in Fig. 6 (approximately the interval between the "Fe" and "Cu" symbols in the A–A′ traverse). Dashed line B–B′ is in the undiseased sphalerite, but the actual position of the traverse lies out of the field and is projected back along strike; as with A–A′, B–B′ is much longer than the segment shown in Fig. 5a. The dark smudges near B–B′ are pits in the polished surface. Field width, 0.150 mm; specimen PBB (31) from Creede, Colorado. (*b*) Bimodal chalcopyrite disease, transmitted light. Black line shows the position of the microprobe traverse plotted in Fig. 8. The semicircular solid black spot cut by the traverse near the bottom of the field is a crystal of chalcopyrite. Field width, 0.30 mm; specimen 79-SK-008 from the Shakanai mine, Hokuroku district, Japan. (*c*) Dusting of chalcopyrite along a fracture in sphalerite; clear sphalerite fills the crack. Black line is the microprobe traverse whose analyses are plotted in Fig. 7. Transmitted light; field width, 0.28 mm; specimen from the Iwami mine, Japan. (*d*) Chalcopyrite disease dusting sphalerite along a fracture. A little chalcopyrite also fills the fracture. Reflected light (oil immersion); field width, 0.44 mm; specimen from Park City, Utah. (*e*) Identical field shown in Fig. 3d; transmitted light. (*f*) Network of fractures showing dusting by chalcopyrite disease. This is the same specimen shown in Fig. 5d and 5e. Transmitted light; field width, 1.03 mm. (*g*) Bead chains in Fe-rich band of sphalerite; the Fe-poor band has no bead chains. Transmitted light; field width, 0.60 mm; specimen PMB-LX from Creede, Colorado. (*h*) Bead chains crossing sector-zone boundary. Thin, lighter color bands within the red sphalerite indicate growth zones. Beads are less abundant in the lighter (lower-Fe) sphalerite. Note irregular bead spacing and gentle curvature of chains. Transmitted light; field width, 0.140 mm; specimen PBB (75) from Creede, Colorado. (*i*) Sphalerite having such fine-grained dusting of chalcopyrite that turbid blue and greenish-yellow colors are produced. Transmitted light; field width, 0.275 mm; specimen from the Magma mine, Superior, Arizona. (*j*) Radiating bead chains in banded sphalerite. The darker horizon to the lower right is parallel to the growth banding; growth direction is upward. Circles are bubbles in the mounting medium. Transmitted light; field width, 1.0 mm; specimen PMB-LX from Creede, Colorado. (*k*) Angular bead chains essentially normal to growth banding. Color change along individual growth bands is related to sector zoning. Note virtual absence of beads in most light-colored sphalerite. Despite the color differences, both the light and dark bands of this sphalerite have about the same concentration of Fe. Transmitted light; field width, 0.20 mm; specimen PMB-BN from Creede, Colorado.

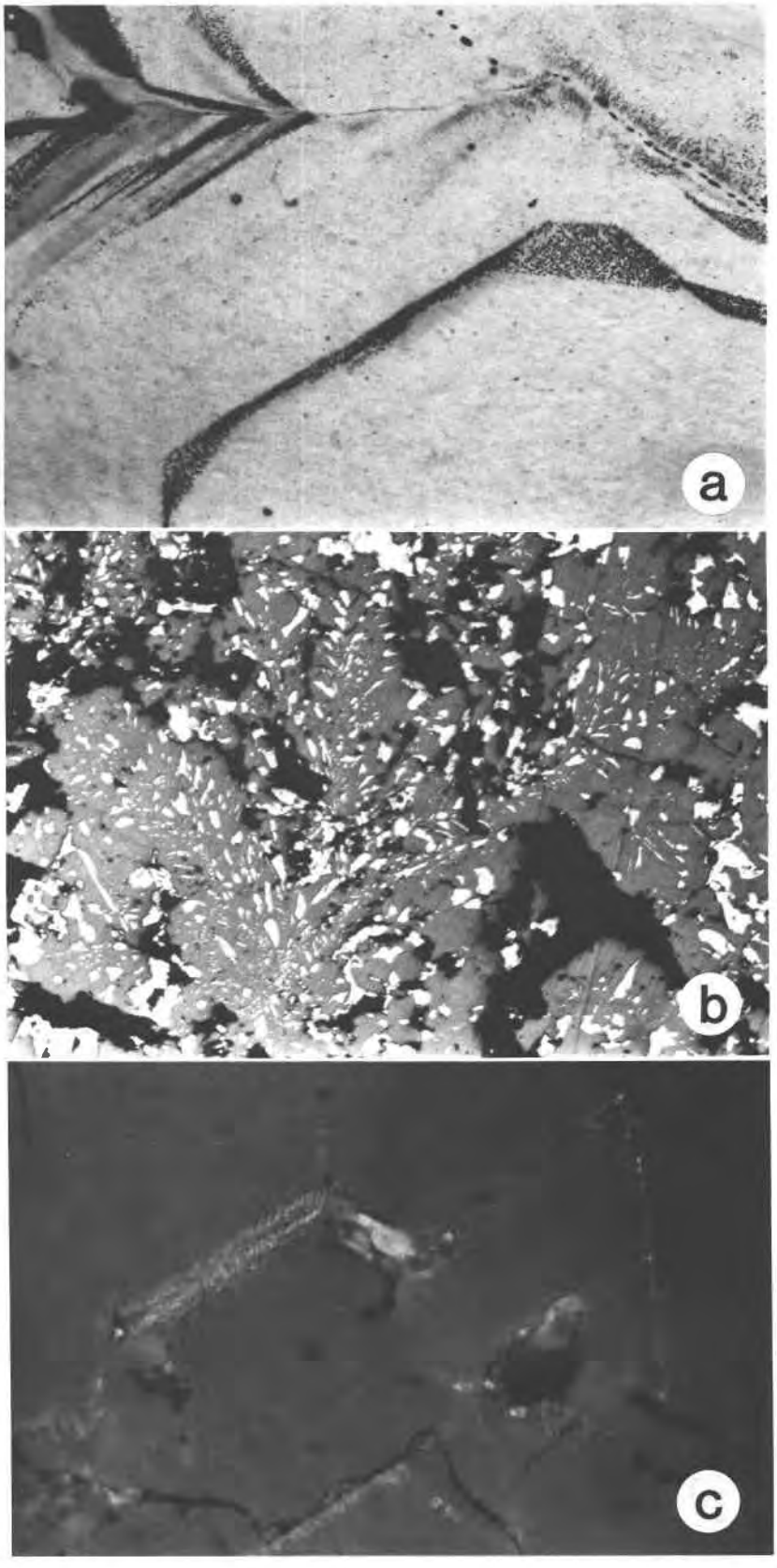

Fig. 9. (*a*) Photomicrograph of an orchard texture of fine chalcopyrite along a former crystal face in sphalerite. See discussion in text. Transmitted light; field width, 1.1 mm; specimen PMB-LX from Creede, Colorado. (*b*) Photomircrograph of coprecipitated chalcopyrite and sphalerite. Reflected light; field width, 2.2 mm; specimen 79HW003A from the Hanawa mine, Japan. (*c*) Photomicrograph of synthetically cultured chalcopyrite disease replacing a single Fe-rich band in growth-banded sphalerite. Reflected light; field width, approximately 1 mm; synthesized and photographed by S. C. Eldridge and others.

similar orchards seem to have advanced along a now-fossil crystal face into clean sphalerite from a grain boundary. Thus orchard texture might even constitute another aspect of the chalcopyrite disease.

Often a few crystals of chalcopyrite that nucleated epitaxially may continue to grow along with the host sphalerite, sometimes forming mutually interfering intergrowths, as Figure 9b shows. Here is an example of synchronous growth from the Hanawa Kuroko deposit, and we note coarse, intergrown skeletal crystals of sphalerite and chalcopyrite that evidently grew upward as a spiny, multibranched plume. Subsequently the aggregate was dusted by the chalcopyrite disease. This texture is typical of the sphalerite + chalcopyrite lining the chimneys of the "smokers" recently discovered so widely along the active spreading axes of the oceanic ridges and from the Troodos ophiolite of Cyprus.

We do not believe that any of these co-depositional situations applies to the three varieties of chalcopyrite disease discussed so far, because we have seen clear and unequivocal evidence that the disease crosscuts the growth banding.

Exsolution is the commonly accepted explanation for textures whose expression in reflected light at least superficially resembles the chalcopyrite disease. Extensive experimental studies, first by Wiggins and Craig (1980), then by Hutchison and Scott (1981), and most recently two studies by Kojima and Sugaki (1984, 1985), all clearly show that the equilibrium solubility of CuS in sphalerite in the Cu-Fe-Zn-S system is *far too low* to explain the amounts of chalcopyrite commonly found intergrown with sphalerite. Figure 10 shows the maximum extent of the sphalerite field for 300 and 700°C in the CuS-FeS-ZnS plane in which sphalerite compositions lie. The quaternary phase relations are quite complex, showing at least a dozen Cu-Fe-S phases coexisting with sphalerites of various compositions; that is the reason for the bumpy character of the outline of the sphalerite field. The numbers enclosed in hexagons indicate the approximate volume percent chalcopyrite in mechanical mixes of chalcopyrite with low-Fe sphalerite.

The important point here is that FeS is soluble in the sphalerite up to where about half of the Zn is replaced by Fe. In contrast, almost no CuS is soluble in sphalerite except in the presence of FeS, and even then, to the extent of only a few mole percent (see Fig. 10). Many of the diseased sphalerite + chalcopyrite intergrowths contain several times more Cu than is available from CuS in solid solution in the one-phase sphalerite field, regardless of the temperature.

One might appeal to a disequilibrium model wherein exsolution occurred from a sphalerite that initially precipitated from a solution highly supersaturated with respect to chalcopyrite. However, microprobe analyses of the interfaces between diseased and healthy sphalerite show appreciable Cu only in the diseased sections, never in the healthy. Thus, both on the grounds of experiment and of microprobe analysis, isochemical exsolution is not

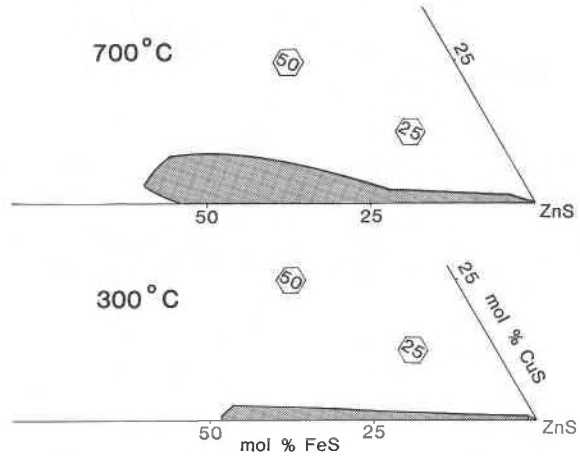

Fig. 10. Isothermal sections for 700 and 300°C of the CuS-FeS-ZnS plane in the Cu-Fe-Zn-S system showing the maximum extent of the sphalerite one-phase field (shaded). Data are taken from Wiggins and Craig (1980), Hutchison and Scott (1981), and Kojima and Sugaki (1984, 1985). The numbers in the hexagons indicate the approximate volume percent of chalcopyrite in mixtures of chalcopyrite and low-Fe sphalerite having bulk compositions plotting in the hexagons.

the answer for the watermelon, the dusting, or the bimodal ailments, although we in no way challenge the fact that exsolution *as a process* should be expected whenever sphalerite is annealed after initially being equilibrated with Cu-Fe sulfides at higher temperatures.

We have ruled out simultaneous deposition and exsolution, and certainly the features we show from undeformed Kuroko and vein deposits cannot be due to mechanical mixtures; thus replacement seems inevitable.

In the course of his investigations on the Kuroko deposits, Stewart Eldridge encountered many examples of the chalcopyrite disease. Together with W. Bourcier, H. Barnes, and H. Ohmoto, he conducted several experiments in which the dusting type of chalcopyrite disease was successfully cultured as a selective replacement of Fe-rich bands in chalcopyrite-free, growth-banded sphalerite (Bourcier and others, 1984). A photomicrograph of their synthetic dusting texture has been contributed by Eldridge and is shown in Figure 9c. The fine-grained chalcopyrite is developed along a favorable (Fe-rich) horizon whereas the less Fe-rich zones are unreplaced.

Among other things, Eldridge and coworkers found that if the Cu content of the solution was too high, that is, the system was too far supersaturated in all of the Cu sulfides, they got only massive replacement of sphalerite by "chalcocite," resembling the products of supergene enrichment. Only when the level of supersaturation was low did the selective partial replacement typifying the disease emerge. Their experiments thus provide a clear demonstration that such replacement can occur and that it can be selective rather than wholesale. Even though we have not resolved the diffusion versus nondiffusion paradox, we are forced to accept replacement.

TABLE 3. Possible chalcopyritization reactions

		Volume change (solids, %)
1.	$Zn_{0.95}Fe_{0.05}S + 0.04Cu^{+} + 0.04H^{+} \rightarrow 0.92Zn_{0.99}Fe_{0.01}S + 0.04CuFeS_2 + 0.02H_2 + 0.04Zn^{2+}$	−0.75
2.	$2ZnS + Fe^{2+} + Cu^{+} + H^{+} \rightarrow CuFeS_2 + 2Zn^{2+} + 0.5H_2$	−7.86
3a.	$Zn_{0.95}Fe_{0.05}S + 0.04Cu^{+} + 0.04H_2S \rightarrow 0.96Zn_{0.99}Fe_{0.01}S + 0.04CuFeS_2 + 0.04H^{+} + 0.02H_2$	+3.2
3b.	$Zn_{0.95}Fe_{0.05}S + 0.04Cu^{+} + 0.04SO_4^{2-} + 0.04H^{+} + 0.14H_2 \rightarrow 0.96Zn_{0.99}Fe_{0.01}S + 0.04CuFeS_2 + 0.16H_2O$	+3.2

Table 3 has a set of possible reactions, each of which might produce the replacement of sphalerite by chalcopyrite. Although written here for specific sphalerite compositions, these are generally applicable reactions that can always be balanced, albeit yielding different values for the volume changes involved. Note that these are one-way reactions, not equilibria. Except for Reaction 2, they consume an Fe-rich sphalerite and yield an Fe-poor sphalerite + chalcopyrite.

Reaction 1 conserves Fe and S, and it exchanges Cu for Zn. H participates to balance the charges. The volume change for the solid phases is minimal, consistent with the preservation of the original textures.

Reaction 2 is for the total replacement of sphalerite by chalcopyrite. It has no mechanism for selective replacement, and it involves a substantial reduction in volume.

The two variants of Reaction 3 each involve the addition of S as well as Cu, while conserving both Fe and Zn in the original sphalerite. 3a and 3b differ only in that one consumes H_2S whereas the other consumes SO_4^{2-}. The H shows up on opposite sides of the reaction to balance the redox change involved in the alternative S sources. Each has a modest volume increase.

We favor Reaction 1. It is driven by the competition for FeS between the ZnS component of sphalerite, which seeks to form an Fe-bearing solid solution, and Cu+ ion, which seeks to react with the FeS to form chalcopyrite.

If S were in short supply, the competition for the available S might be between Zn on one hand and Cu and Fe on the other, and the massive replacement of sphalerite by chalcopyrite represented by Reaction 2 would prevail. If S were even more limited, then we would expect chalcocite as the product, as occurs in the supergene environment.

We do not see justification to appeal to either reactions 3a or 3b to explain the chalcopyrite disease.

The three aspects that we have described so far constitute the chalcopyrite disease proper, but there are at least three additional features that may constitute related miseries; see Table 4. Two of these we have lumped under the name "bead chains," and the interpretation of them as replacement is probably unwarranted because the chalcopyrite in them constitutes so small an amount of Cu that it might, indeed, be derived from possible sphalerite solid-solution compositions.

TABLE 4. Various aspects and probable causes of the chalcopyrite disease

1. Watermelon 2. Dusting 3. Bimodal	Replacement
4. Bead Chains 5. Angular-bleb Bead Chains	Exsolution
6. Veils (probably not part of the chalcopyrite disease syndrome)	

BEAD CHAINS

Bead chains may, or may not, represent a phenomenon related to the previously discussed replacement features, but we discuss them here as aspects of the chalcopyrite disease because they occur in similar materials and because they all share the diffusion versus nondiffusion enigma. Bead chains are very numerous in some parts of some crystals and may be entirely absent in other parts of the same growth band in the same crystal. One of the very best specimens displaying bead chains has already been noted (Fig. 2i) where they are certainly not at all obvious at the approximately 1.5× magnification used in that illustration. They are best developed in moderately Fe-rich sphalerite (perhaps 2 to 5 or 10 mol% FeS) and rare to absent in lower-Fe material. The bead chains constitute so small a volumetric proportion of the sphalerite crystals that they are below resolution by most bulk analytical techniques. They can be very obvious to microscopic examination, but we are also continually amazed by how many critical observations one can ignore when one does not know what to look for.

Examination at low magnification of doubly polished plates of sphalerite often shows numerous apparent "scratches" *within* the crystals. Figure 5g shows hundreds of these features starting just where an upward-growing sphalerite crystal changes from very low to moderate Fe content and becomes visibly banded; the chains are arrayed primarily normal to the growth surface of the crystal.

Closer study (Fig. 11a) shows that the interior "scratches" are actually arrays of inclusions that are often connected by scarcely visible "threads." We have given these features the descriptive name of "bead chains," and as a working hypothesis we shall follow Ed Roedder's suggestion that they form as decorated crystal defects, a well established phenomenon observed in many minerals.

Some individual chains may be followed continuously for tens of millimeters! In the rare instances where the inclusions are seen to crop out on the polished surface, they seem to be chalcopyrite although they are far too small for definitive optical or microprobe analysis. All too frequently, only tiny voids are visible; these we interpret to be the roots of inclusions from which the chal-

copyrite has been plucked during section preparation. There remains a small possibility that some of the inclusions are voids instead of solid. Bead chains are difficult to photograph because an adequate magnification leads to such a loss of depth of field that one cannot clearly see the entire texture.

Examination of Figure 11 shows that the beads on the chains are highly varied in size. They range downward from rare giants having diameters of several micrometers down to at least the limit of optical detection at ~0.1 μm. There are surprising contrasts in sizes of beads in adjacent chains; Figure 11n is a good example. Those inclusions greater than ~1 μm often show platelike morphology, the plates being oriented systematically with respect to the host sphalerite. In Figure 11l and 11m, the plates alternate through several orientations. Except for the plates, most beads appear equant and rounded, although they may be so closely strung as to constitute lumpy rods.

Of even more variability is the way inclusions are related to each other, both within individual chains and between chains. An isolated row of inclusions is rare; usually one sees dozens at a time and usually they are parallel to subparallel. But they do intersect, curve, and branch, as in Figure 11j or as in Figures 11f and 11h that display perfect tetrahedral figures a few tens of micrometers on an edge. It is not uncommon to observe several chains of inclusions emanating from a solid inclusion, such as, in the instance of Figure 11d, a hematite flake. Once in a while, as in Figure 5j, there seems to be a festival going on, with whole armadas of bead chains shooting off fireworks in unison. When branching of chains is observed, it usually occurs in the direction of crystal growth, but forms such as the tetrahedra noted above constitute a special exception.

Although most of the bead chains are linear and normal to growth surfaces, they do exhibit both rigid and erratic geometric forms, as shown in Figure 11c; this bramble patch is only a millimeter away, and in the identical growth zone, from a perfectly orderly, well-combed set of chains like those shown in Figure 5g. Figure 11b shows a pair of orderly, continuous chains, whereas a few micrometers away, a scattered formation of beads seems unable to get its act in order. In Figure 11i, one chain of a parallel triad suddenly goes off on its own. Figure 11g illustrates diversity in bead spacing among many nearly parallel chains; a few show cusps. In Figure 11e, one of many chains does a "U turn," but the rest go straight through; actually, the "U turner" has a mirror-image counterpart in the darker sphalerite just to the left of the label. Obviously, each marches to its own drummer!

Some chains contain beads that are themselves composites of a larger central inclusion plus numerous smaller satellitic beads, all of which are of similar size and lie more or less on the same circle centered on the large bead (Figs. 11k, 11o, and 11p). In a few instances (Figs. 12a and 12b), we have noted accessory sets of hairlike, planar loops, a few micrometers across, emerging like microscopic wings from bead chains. The loops in Figure 12 are small-scale bead chains, but sometimes the loops carry no beads. Figure 12b has unusually coarse beads in the main chain, and the complex beaded loops strongly resemble incompletely healed fractures.

One very important aspect of these bead chains is their irregular occurrence. In beautiful crystals such as the one in Figure 2i we commonly find the chains in the darker, more Fe-rich bands; at least, the chains are better decorated by beads there even though they may continue cryptically through the paler sphalerite. However, in some of the sector-zoned crystals we note that the bead chains are confined to certain sectors and that other sectors, representing the same growth band and having very similar optical characteristics, may have no bead chains at all. Usually the frequency of beads along the chain decreases markedly as the chain is followed into less Fe-rich sphalerite (Fig. 5h), but several of the photomicrographs demonstrate that the chains can continue unabated into a less Fe-rich host. Figure 2h also presents us with a problem in that the bead chain seems to be crossing a sector-zone boundary. If sector zones represent portions of the crystal that grew from different crystal forms, why should a defect propagate itself across the interface?

The inclusion chains disappear as they approach within a few tens of micrometers of large primary fluid inclusions, but extensive measurements on fluid inclusions by Roedder (1977) and Hayba (1984) have conclusively demonstrated that the chains are not a cause of leakage. Both investigators noted that the fluid inclusions had a very systematic salinity and temperature pattern that followed closely the optically visible growth banding of the host sphalerite despite the fact that crosscutting bead chains were abundant. This lack of diffusion of fluids along bead chains is one argument that the beads do not originate by a mechanism requiring the chains to function as pipelines.

In no instance have we observed a bead chain terminating outward in a large chalcopyrite inclusion of the sort suggestive of co-deposition with the sphalerite. Nor is there any evidence (such as preferential development below microkarstic disconformities) that they become decorated *during* crystal growth. They must be formed subsequent to the growth of the enclosing sphalerite.

Almost inevitably we must conclude that the bead chains are decorated growth defects, possibly the axes of spiral dislocations, or perhaps the intersection between three spirals. If this is so, then they have a good deal more to tell us about the growth of the sphalerite crystals than we have yet deciphered.

We attribute the decoration of the defects to the local exsolution of CuS and FeS to yield chalcopyrite. This interpretation is consistent with the facts that the levels of Cu necessary to form the beads (a few hundred ppm would probably suffice) could certainly escape detection by microprobe and that cooling (or even re-equilibration of metastably incorporated Cu) could lead to exsolution

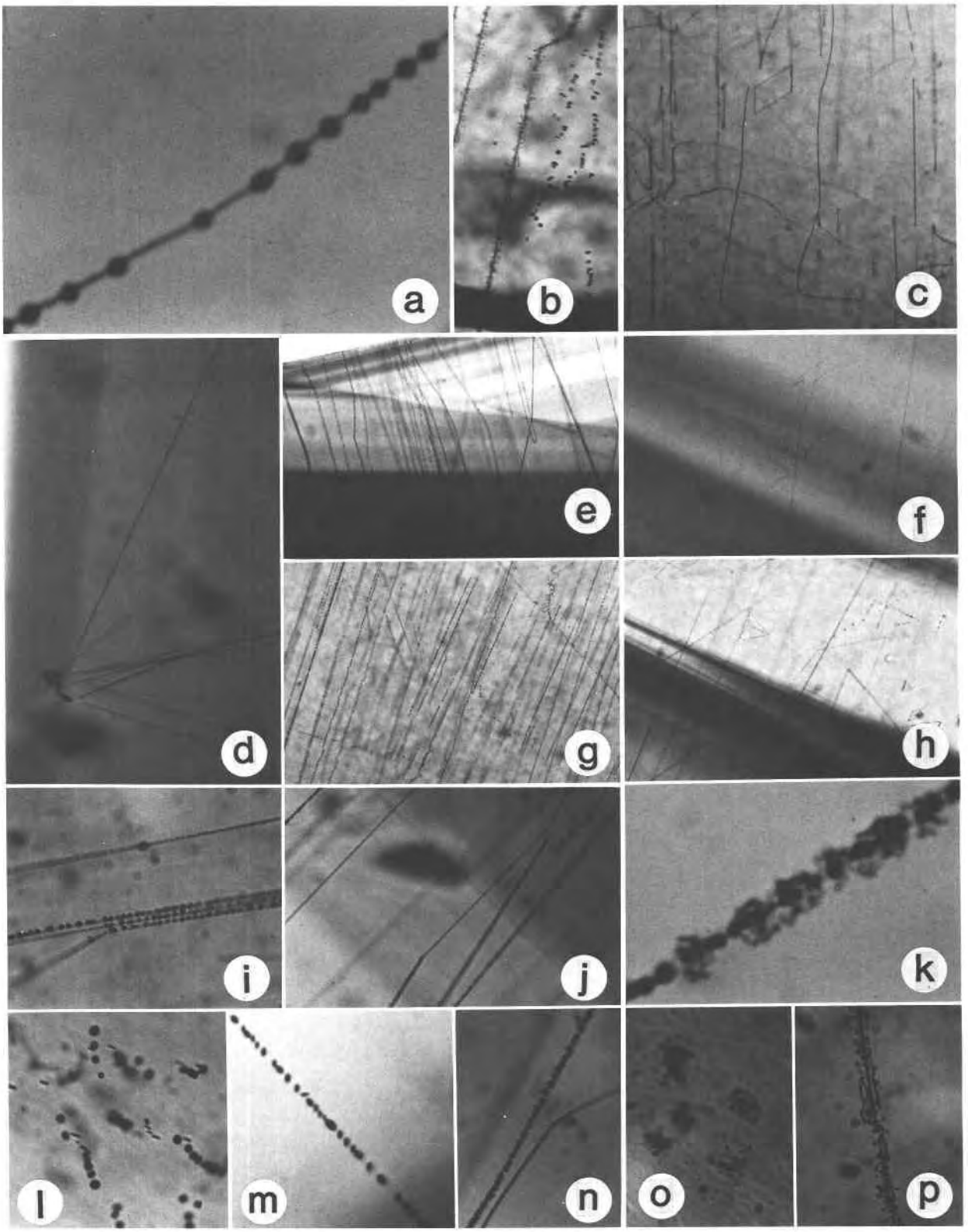

Fig. 11. Collage of photomicrographs showing bead chains in sphalerite from Creede, Colorado. All photomicrographs in transmitted light. (*a*) Close-up of typical bead chain; field width, 0.025 mm; specimen PMB-AK. (*b*) Contrasting spacing, size, and alignment of beads in adjacent bead chains; field width, 0.17 mm; specimen PBB (75). (*c*) Contorted bead chains; field width, 0.60

on a micrometer scale. But why are just some areas affected, while similar-appearing crystal sectors elsewhere in the same crystal escape bead formation? Since the Fe content is always far, far higher than is necessary to supply the FeS for contained bead chains, and since we can call only on exsolution as a practical explanation for these features, we suspect that the Cu is strongly sector-zoned and that given a better mode of analysis we might find that the bead-bearing sectors are indeed richer in primary Cu.

The beads with satellitic halos might be candidates for exsolution through annealing from the so-called "Cottrell atmosphere," which is a local concentration of impurity components in the vicinity of defects (Cottrell, 1948). The Cottrell atmosphere is principally a theoretical concept with little direct observational evidence (but see Kitamura and others, 1986). We cannot carry this interpretation further except to note that the formation of a bead chain requires a 300-fold (or more) concentration of Cu from the sphalerite into the chalcopyrite; this implies a source volume having a radius of at least 5 times (and probably 10 or 20 times) that of the bead to supply enough Cu. The bead chains therefore present a diffusion versus nondiffusion dilemma similar to that for the watermelon texture.

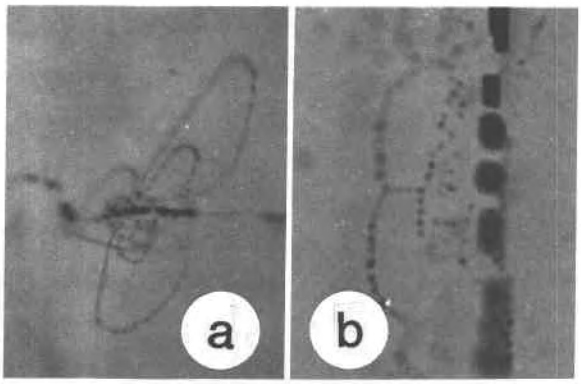

Fig. 12. Bead chains with accessory loops; samples from Creede, Colorado. (*a*) Bead chain with closed, decorated accessory loops. Field width, 0.055 mm; photo by E. Roedder. (*b*) Bead chain with unusually coarse beads and closed, decorated double loops. The origin of this unusual feature is problematic. Field width, 0.023 mm; photo by E. Roedder.

Angular-bleb bead chains

The second variety of bead chains is designated the "angular-bleb bead chains." This feature is often associated with a peculiar pinkish-brown (which photographs as just a garden-variety brown, Fig. 5k) sphalerite that is sharply controlled by twin planes within individual sphalerite crystals and, therefore, may be thought of as a feature related to sector zoning. Figure 5k shows an example in which the beads show a strong preference for the darker sphalerite although the defects presumably continue straight through all sectors.

One peculiar feature is that the Fe content of the pinkish-brown host is at a similar low level to that of the surrounding colorless or yellow sphalerite. Although the angular-bleb bead chains highly prefer the pinkish-brown host, they are not responsible for the peculiar color because the pinkish-brown sphalerite sometimes occurs without any bead chains. As with the ordinary bead chains, a detailed examination of the distribution of trace Cu concentrations would be most interesting.

In the angular-bleb bead chains, the chalcopyrite has a coarser grain size, perhaps about $5 \times 5 \times 1$ μm, than any other disease-related chalcopyrite except the watermelon seeds. In most instances the chalcopyrite in the angular-bleb bead chains occurs as blocky euhedra. Note that the bead chains constitute nearly linear features that trend approximately normal to the growth surfaces and that the beads are not exactly aligned but rather seem to wobble a bit about an axis. Although the angular-bleb bead chains are quite common, we have not observed them performing the same gyrations as do the ordinary bead chains. Most examples of angular-bleb bead chains consist of only them; however, Figure 11b is strongly suggestive that both varieties of bead chains may coexist in close proximity.

Veils

Finally, there are numerous examples of very fine inclusions, some unknown fraction of which may be chalcopyrite, distributed in linear arrays that usually are at a high angle to the crystal-growth surfaces, usually parallel to twin planes. We refer to these wispy features as "veils."

←

mm; specimen PMB-CC. (*d*) Bead chains radiating from hematite inclusion; the crystal grew from left to right. Field width, 0.26 mm; specimen PMB-AK. (*e*) A variety of bead chains in sphalerite. Field width, 0.66 mm; specimen PBB (75). (*f*) Bead chains outlining a perfect tetrahedron; field width, 0.30 mm; specimen PMB-AK. (*g*) A variety of bead chains. Field width, 0.66 mm; specimen PMB-CC. (*h*) Bead chains outlining tetrahedra; the largest one is just above and left of the center of field; another smaller tetrahedron is just above label. Field width, 0.66 mm; specimen PBB (75). (*i*) A variety of bead chains; field width, 0.11 mm; specimen PBB (75). (*j*) Intersecting and irregularly decorated bead chains; field width, 0.33 mm; specimen PMB-AK. (*k*) Bead chains with satellitic halos; field width, 0.018 mm; specimen PMB-AK. (*l*) Different orientations of platelike chalcopyrite beads; field width, 0.089 mm; specimen PMB-HJ. (*m*) Different orientations of platelike chalcopyrite beads; field width, 0.089 mm; specimen PMB-AK. (*n*) Contrasting bead chains; field width, 0.066 mm; specimen PMB-AK. (*o*) Isolated beads with satellitic halos; field width, 0.066 mm; specimen PMB-HJ. (*p*) Bead chains with irregular satellitic halos; field width, 0.066 mm; specimen PBB (75).

These are the only features mentioned that we have noted in low-temperature deposits of the Mississippi Valley type. They may well be simply growth defects decorated or marked by a variety of inclusions and in no way related to the chalcopyrite disease. We shall not discuss them further here.

Epidemiology

Now that we have described the symptoms, let us touch lightly again on the epidemiology of the chalcopyrite disease.

We have seen the chalcopyrite disease, especially the dusting aspect, in most unmetamorphosed hydrothermal vein deposits that we have examined, and in all of the Kuroko deposits and modern, sphalerite-bearing, oceanic spreading–ridge "smoker" deposits. H. Shimazaki (1986, and pers. comm.) has noted similar features in skarns from Japan and Korea. We have never seen the disease in any of dozens of sections from Mississippi Valley–type deposits.

It seems to occur in moderate temperature, i.e., 200 to 400°C, deposits that are formed and "quenched" in a geologically brief time. Metamorphism homogenizes the sphalerite banding, recrystallizes both the chalcopyrite and its host sphalerite, and coarsens the textures thereby masking its heritage. In fact, Scott (1983) called on the recrystallization of diseased sphalerite to account for occurrences of sphalerite with abundant chalcopyrite inclusions in metamorphosed ore deposits. We agree with Scott, in part, but an attractive alternative would be that the high initial chalcopyrite concentration is provided by coprecipitation textures such as that shown in Figure 9b.

What next?

As we indicated in the introduction, many interesting questions regarding this ailment are open for additional research. Perhaps most prominent among the many possible avenues would be the application of transmission electron microscopy to all of the textures, but most especially the bead chains. Another promising experiment would be to etch the surfaces that intersect the bead chains and examine them for evidence of growth mechanisms by scanning electron microscopy.

Some additional targets for research include looking for phases other than chalcopyrite as inclusions; we have already observed rare occurrences of tetrahedrite and galena in place of chalcopyrite in the epithermal and Kuroko environments and tentatively have relegated them to replacements of chalcopyrite blebs. We might look for bornite or chalcocite as suggested by the studies of Dickinson and Pattrick (1986), although their findings in this regard seem more likely to us to be related to supergene processes. We might also ask why we have not observed pyrite blebs of similar origin forming in a Cu-deficient environment in response to an increase in S activity.

A study of fluid inclusions in host and diseased regions would be particularly informative, but we have not found very many inclusions of unquestioned primary origin in this material and have not gathered that information as yet.

In closing, let us again summarize the chalcopyrite ailment; it has several aspects that we must attribute to different processes, particularly solid-state replacement for the watermelon, dusting, and bimodal textures and exsolution for the bead chains. Whether or not these principal catagories are related to a common virus is indeterminant today. These volumetrically trivial features are all transitory, occurring as crystals attempt to achieve equilibrium with their external and internal environments. However, they are responsible for some significant problems in mineral beneficiation, and they do have the potential to indicate something about the rates of crystal-chemical processes and about the postdepositional thermal history in a variety of ore deposits.

Note added in proof: Sugaki and others (1987) have recently described the bulk compositions of sphalerite containing minute blebs of chalcopyrite from a variety of Japanese deposits. The bulk compositions they have reported are well outside of the one-phase sphalerite stability field, and they have concluded, in complete agreement with our study, that a process other than exsolution must be responsible.

Acknowledgments

We have shown these textures to everyone who would permit themselves to be dragged to our microscope. Most observers have shared our awe and inability to explain them. We nonetheless appreciate their many questions and arguments that often have forced us to look again yet one more time. E. Roedder in particular has contributed many pertinent observations and useful suggestions; he also joined with H. Evans in providing much appreciated reviews. We greatly appreciate the sharing of as yet unpublished data by C. S. Eldridge and H. Shimazaki. The term "chalcopyrite disease" is the result of J. R. Craig's terse commentary noted above. We would particularly like to thank the Mineralogical Society of America, which, through its Council, permitted us to include the color plates, without which this tale would have been rather drab.

References

Barton, P.B., Jr. (1978) Some ore textures involving sphalerite from the Furutobe mine, Akita Prefecture, Japan. Mining Geology, 28, 293–300.

Bourcier, W.L., Eldridge, C.S., Barnes, H.L., and Ohmoto, H. (1984) The chalcopyrite disease in Kuroko ore: An experimental investigation. Geological Society of America Abstracts with Programs, 16, 452.

Cottrell, A.H. (1948) Report on the strength of solids. The Physical Society, London, p. 30.

Dickinson, C., and Pattrick, R.A.D. (1986) Electron microscopic investigation of sphalerite and sphalerite-chalcopyrite intergrowths. International Mineralogical Association Abstracts with Program, 89.

Eldridge, C.S., Barton, P.B., Jr., and Ohmoto, H. (1983) Mineral textures and their bearing on the formation of the Kuroko orebodies. Economic Geology Monograph 5, 241–281.

Hayba, D.O. (1984) Documentation of thermal and salinity gradients and interpretation of the hydrologic conditions in the OH vein, Creede, Colorado. Geological Society of America Abstracts with Programs, 16, 534.

Hutchison, M.N., and Scott, S.D. (1981) Sphalerite geobarometry in the system Cu-Fe-Zn-S. Economic Geology, 76, 143–153.

Kitamura, M., Matsuda, H., and Morimoto, N. (1986) Direct observation

of the Cottrell atmosphere in olivine. Proceedings of the Japan Academy, 62, Series B, 140–152.

Kojima, S., and Sugaki, A. (1984) Phase relations in the central portion of the Cu-Fe-Zn-S system between 800° and 500°C. Mineralogical Journal, 12, 1528.

——— (1985) Phase relations in the Cu-Fe-Zn-S system between 500° and 300°C under hydrothermal conditions. Economic Geology, 80, 158–171.

McLimans, R.K., Barnes, H.L., and Ohmoto, H. (1980) Sphalerite stratigraphy of the upper Mississippi Valley zinc-lead district: Southwest Wisconsin. Economic Geology, 75, 351–361.

Roedder, E. (1977) Changes in the ore fluid with time, from fluid inclusion studies at Creede, Colorado. Problems of Ore Deposition, Fourth IAGOD Symposium, 1974, Varna, vol. 2, 179–185.

Scott, S.D. (1983) Chemical behavior of sphalerite and arsenopyrite in hydrothermal and metamorphic environments. Mineralogical Magazine, 47, 427–435.

Shimazaki, H. (1986) "Chalcopyrite disease" in sphalerites (abs.). Mining Geology, 36, 63 (in Japanese).

Sugaki, A., Kitakaze, A., and Shima, S. (1987) Bulk compositions of intimate intergrowths of chalcopyrite and sphalerite and their genetic implications. Mineralium Deposita, 22, 26–32.

Wiggins, L.B., and Craig, J.R. (1980) Reconnaissance of the Cu-Fe-Zn-S system: Sphalerite phase relationships. Economic Geology, 75, 742–751.

Manuscript received February 5, 1987
Manuscript accepted February 16, 1987